Journal of Magnetic Resonance **143,** 197–207 (2000)
doi:10.1006/jmre.1999.1966, available online at http://www.idealibrary.com on IDEAL®

ω-Space Adaptive Acquisition Technique for Magnetic Resonance Imaging from Projections

G. Placidi,*,† M. Alecci,* and A. Sotgiu*

**INFM, % Department of Biomedical Sciences, University of L'Aquila, Via Vetoio 10, 67100 L'Aquila, Italy; and †Department of Electrical Engineering, University of L'Aquila, Roio Poggio, 67100 L'Aquila, Italy*

Received July 20, 1999; revised October 22, 1999

An ω-space adaptive acquisition technique for MRI from projections is presented. It is based on the evaluation of the information content of a set composed of four initial projections, measured at angles 0°, 45°, 90°, and 135°, followed by the selection of new angles where the information content is maximum. An entropy function is defined on the power spectrum of the projections that is useful for evaluating the information content of each projection. The method makes it possible to reduce the total acquisition time with little degradation of the reconstructed image and it adapts to the arbitrary shape of the sample. For this reason, it can be particularly useful in those applications where acquisition from projections is strongly recommended to save acquisition time, such as functional MRI, imaging of species having very short T_2, or angiography. The method has been tested both on simulated data and on experimental data collected by a commercial MRI apparatus. The method has also been compared to the regular acquisition method, that is, the standard acquisition method in MRI from projections.

INTRODUCTION

Although reconstruction from projections, RP (*1*), was the first technique employed in magnetic resonance imaging (MRI), it has been substituted by the so-called Fourier transform methods, FT (*2–6*). Nevertheless, RP has been recently revaluated because of some of its important properties. In particular, it is less sensitive to the effects of movement than the FT methods. The artifacts due to movement can be very misleading when MRI is used to perform imaging of abdominal regions, being essentially due to breathing. In these applications, acquisition techniques based on FT methods or their variations produce artifacts and distortions principally along the direction of phase-encoding. Possible solutions are FT-based sequences, such as fast spin-echo (*7*), spiral-scan (*8*), or particular applications of echo-planar (*9*), which allow the collection of image data in a short time with respect to physiological movements. However, their use can preclude the utilization of contrast enhancement techniques when the relaxation times are shorter than the acquisition times. Moreover, it results in loss of resolution and signal to noise ratio (S/N). In these cases, acquisition sequences based on RP methods (*10–15*) can be convenient because the acquisition time is reduced by eliminating the phase-encoding step. The motion artifacts are also reduced, when using RP, by the fact that the center of the ω-space of the image is oversampled. This fact implies an increase of the S/N ratio of the image when compared with that obtained by FT methods. Moreover, the center of the ω-space is obtained at the start of the reading time, thus eliminating from the central zone motion artifacts affecting the last period of the reading interval. Another advantage of RP methods is the possibility of collecting just half of the data required to reconstruct an image (*16, 17*); in this way the acquisition time can be further reduced.

For these reasons, RP methods are widely used to perform imaging of species having very short T_2 (*18, 19*) or in angiography where it is important to reduce the artifacts due to blood flow (*20, 21*). Thanks to these important qualities, a great number of acquisition sequences support acquisition from projections (*16, 21–23*). Some sequences have taken advantage of the reduction of acquisition time to perform dynamic functional studies of some parts of the human body, such as joints (*23*). In these applications, the reduction of acquisition time is very important and the gain in the reconstructed image is proportional to the time saved. Nevertheless, there are some temporal limits, both instrumental and physical, that are impossible to overcome further by means of any acquisition technique, whether based on FT or RP methods. In fact, there is a lower limit to the acquisition time per projection and to the minimum number of projections to reconstruct an image of given dimensions (*24*). This is true if nothing is known about the sample or if the sample does not contain internal symmetries. However, it is possible to reduce the number of projections if intrinsic properties of the sample can be used.

In the context of continuous wave electron paramagnetic resonance imaging, an adaptive RP acquisition technique has been presented (*25*) that, without any a priori knowledge of the sample, is able to obtain a near optimal set of projections to reconstruct an image without loss of information. This is done by evaluating the information content of the acquired projections using a function called the entropy of the projections. The following projections are collected where the difference in

1090-7807/00 $35.00

information content is greatest. The process ends when the greatest difference is less than an estimated value. This adaptive technique considerably reduces the total number of projections required if the sample contains some structural regularity or symmetry (*24*). Because of the continuous wave acquisition mode, this technique evaluated the information content of the projections in the signal space and not in the ω-space. Its extension to the reconstruction from projections, whose Fourier coefficients are given, would be trivial if we consider the evaluation of the Fourier transform of each projection before the calculation of the entropy function. But, in this case, the whole frequency spectrum of the measured projections is required and the advantage resulting from the reduction of the total acquisition time by using just a few parts of the frequency spectrum is lost.

In the present work, we extend the concept of the entropy of a projection by defining it directly in Fourier space. In this way, the reduction of the total acquisition time by collecting part of the Fourier space is maintained and a further time reduction, resulting from the use of adaptive acquisition, is obtained. In what follows, a full theoretical description of the method is given and the tests of the new technique, both on simulated and on experimental data, are reported. Moreover, a comparison between the regular and optimal ω-space adaptive acquisition techniques is also made.

THEORY AND METHOD

Projection Reconstruction Technique: Background

We suppose that the function $f(x, y)$, defined in a limited two-dimensional (2-D) domain D, represents an image and that $f(x, y) \leq M$ for all $(x, y) \in D$, where M is a real constant. The projection $p_\varphi(r)$ of $f(x, y)$ along the r direction is given by

$$p_\varphi(r) = \int_{-\infty}^{\infty} f(r,s)ds, \qquad [1]$$

where $r = x\cos(\varphi) + y\sin(\varphi)$ and $s = x\sin(\varphi) - y\cos(\varphi)$.

Let

$$p_\varphi(\omega) = \int_{-\infty}^{\infty} p_\varphi(r)\, e^{-2\pi i\omega r} dr \qquad [2]$$

be the Fourier transform of the projection taken at an angle φ. The Fourier terms of the image $f(x, y)$, in polar coordinates, are described by

$$F_\varphi(\omega) = \int_{-\infty}^{\infty}\int_{-\infty}^{\infty} f(r,s)\, e^{-2\pi i\omega r} dr ds$$

$$= \int_{-\infty}^{\infty} p_\varphi(r)\, e^{-2\pi i\omega r} dr$$

$$= p_\varphi(\omega). \qquad [3]$$

MR imaging from projections consists of the following steps: acquire the real and imaginary parts of the Fourier transform of a limited set of radial projections; position them at the right angle positions in the ω-plane, according to Eq. [3]; interpolate to obtain a cartesian grid of Fourier coefficients; calculate the 2-D inverse Fourier transform to obtain the final image.

By calling S_f the sum of $f(x, y)$, at any angle φ, we have

$$S_f = \int_D f(x,y)dxdy = \int_r p_\varphi(r)dr = p_\varphi(\omega_0), \qquad [4]$$

where ω_0 is the central frequency (the DC component). In practical applications, $f(x,y)$ is evaluated at a finite number of pixels, $n*n$, from experimental data measured at a limited number of projections, each sampled at a fixed number of points, n. In this case, the integral of Eq. [4] can be replaced by a sum and, without any loss of generality, the value of S_f can be normalized to $1/n$.

The Entropy Function

Due to the properties of $f(x,y)$ and to the previous assumption, the DC value of each projection is exactly $1/n$ and the amplitude of any other frequency component of each projection is less than, or equal to, $1/n$. This is an important condition and its use will be clear later, when the information content of each projection is defined.

Let $\mathrm{Pw}_\varphi(\omega)$ be the power spectrum of $p_\varphi(r)$, expressed by the relation

$$\mathrm{Pw}_\varphi(\omega) = \mathrm{R}_\varphi^2(\omega) + \mathrm{I}_\varphi^2(\omega), \qquad [5]$$

where $\mathrm{R}_\varphi(\omega)$ and $\mathrm{I}_\varphi(\omega)$ represent the real and imaginary parts of the projection at the angle φ, respectively. To evaluate the information content of different projections by evaluating that of its power spectrum, we introduce the "entropy" $E\mathrm{Pw}_\varphi$ of the power spectrum of a projection as

$$E\mathrm{Pw}_\varphi = \sum_{i=1}^{n} \mathrm{Pw}_{\varphi,i}\log\left(\frac{1}{\mathrm{Pw}_{\varphi,i}}\right), \qquad [6]$$

where $\mathrm{Pw}_{\varphi,i}\log(1/\mathrm{Pw}_{\varphi,i}) = 0$ for $\mathrm{Pw}_{\varphi,i} = 0$ and for $\mathrm{Pw}_{\varphi,i} = 1$.

If, as the base of the logarithm, we take the square of the number of points sampled for each projection, $E\mathrm{Pw}_\varphi$ assumes values between $1/n^2$ and $1/n$. $E\mathrm{Pw}_\varphi = 1/n^2$ corresponds to the case in which the power spectrum of the projection is zero

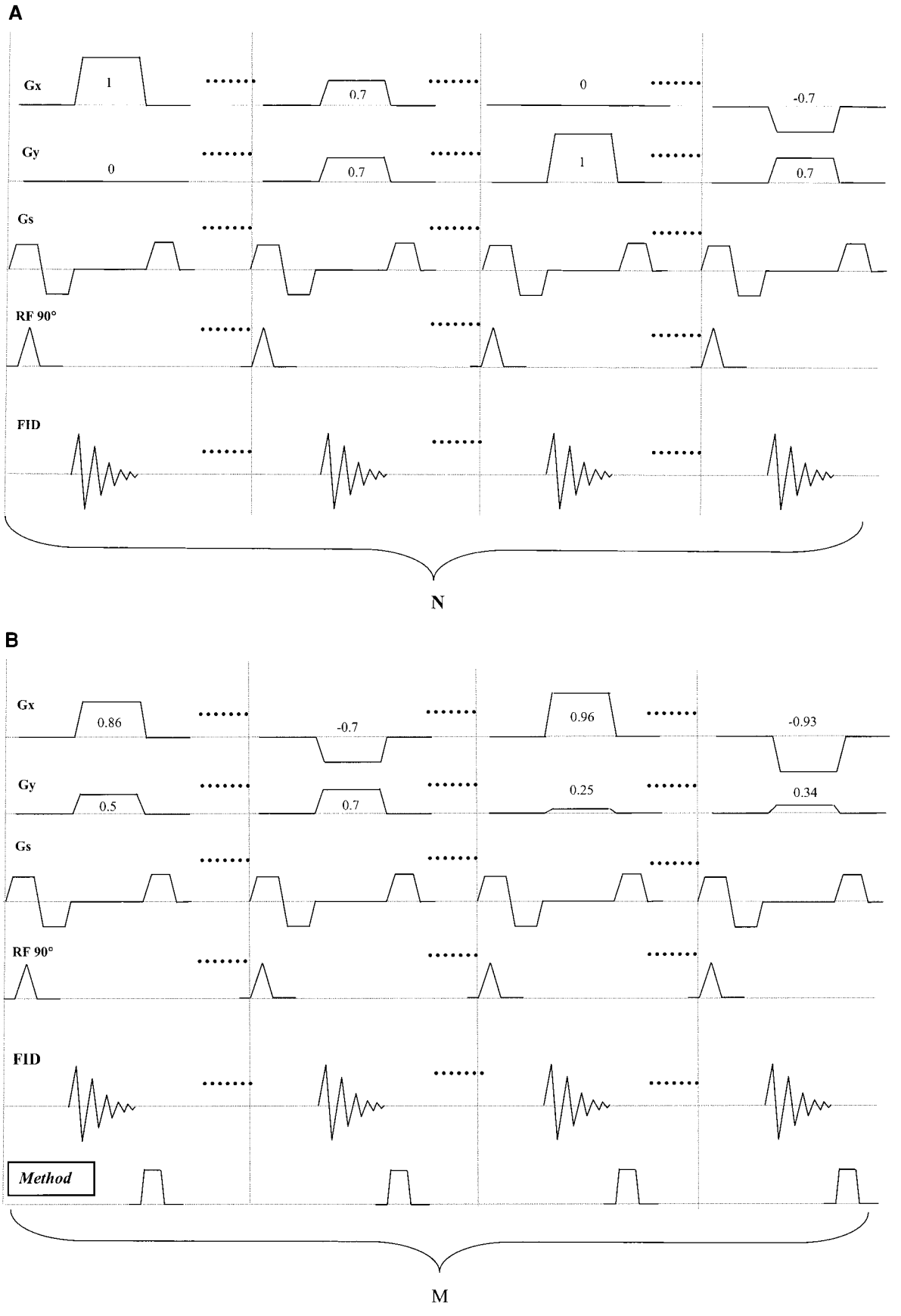

FIG. 1. Example of the application of the regular acquisition sequence (A) and of the adaptive acquisition sequence (B).

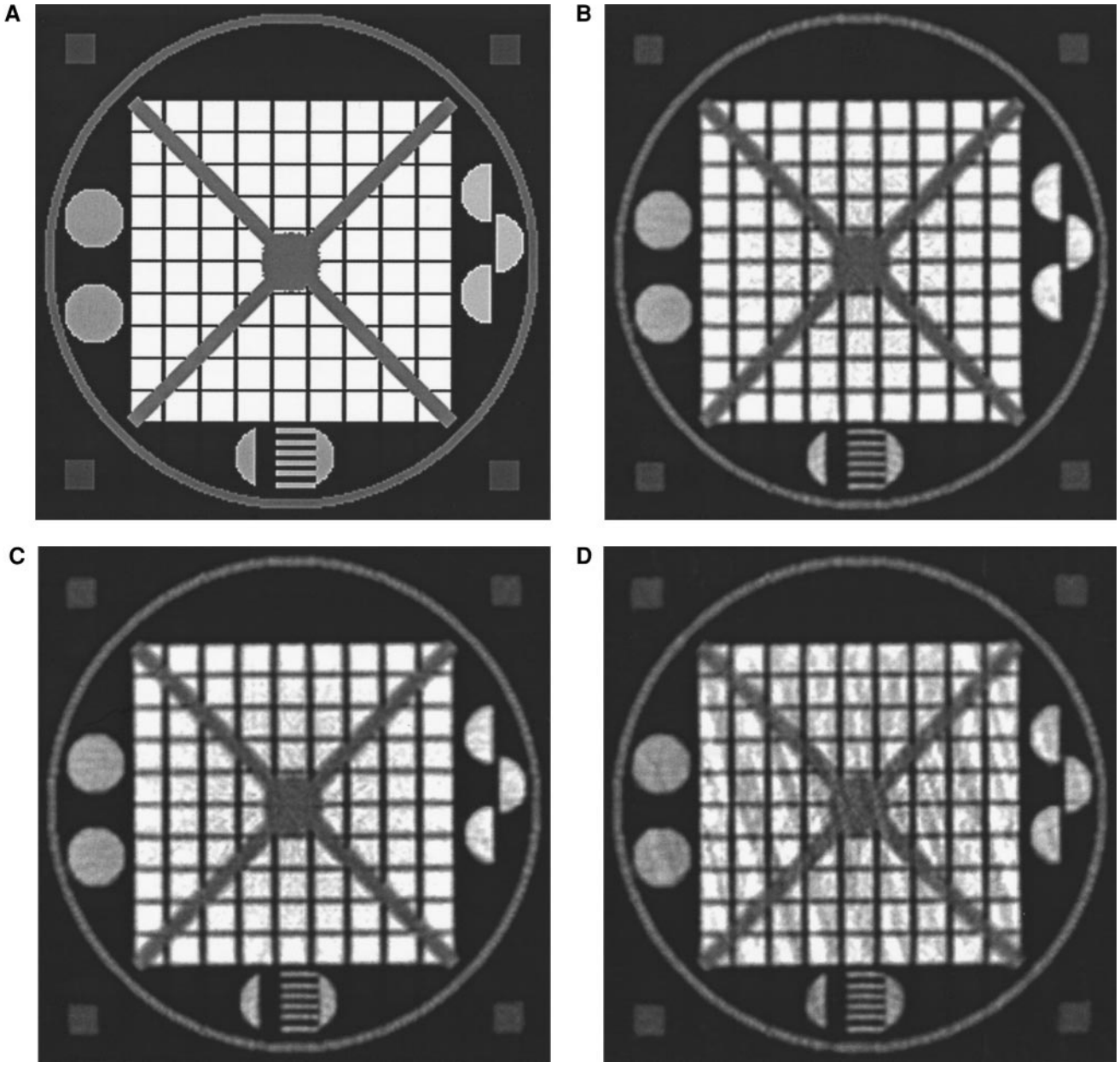

FIG. 2. Digital 256*256 image (A) of an ideal phantom. In (B) the reference image, reconstructed using the whole set (1000) of simulated projections, is reported. The images reconstructed by using 120 projections collected by the adaptive method and 125 and 201 projections collected by the regular method are shown in (C), (D), and (E), respectively.

everywhere with the exception of the DC component at which its value is $1/n^2$. In this case, the projection has constant value everywhere and it has the minimum information content. When all the points of the power spectrum of the projection have the same value, equal to $1/n^2$, then $E\mathrm{Pw}_\varphi = 1/n$ and the projection has the maximum information content. In fact, the projection corresponds to a Dirac δ function (maximum information content). The definition given above represents the dual of the definition of entropy of a projection reported in Ref. (*25*). In fact, both assume that a projection is considered to be more significant when it gives more details of the distribution of $f(x,y)$ and, as seen before, this occurs for greater values of the entropy of the power spectrum of the projection or, equivalently, for lower values of the entropy of the projection (*25*). The function $E\mathrm{Pw}_\varphi$ gives an estimate of the information content that is independent of the observer: it only depends on the shape of the object to be observed.

When data are obtained by sampling a physical process, noise is always present. We suppose that the two signals, the real and imaginary parts of the FT of the projection, have been

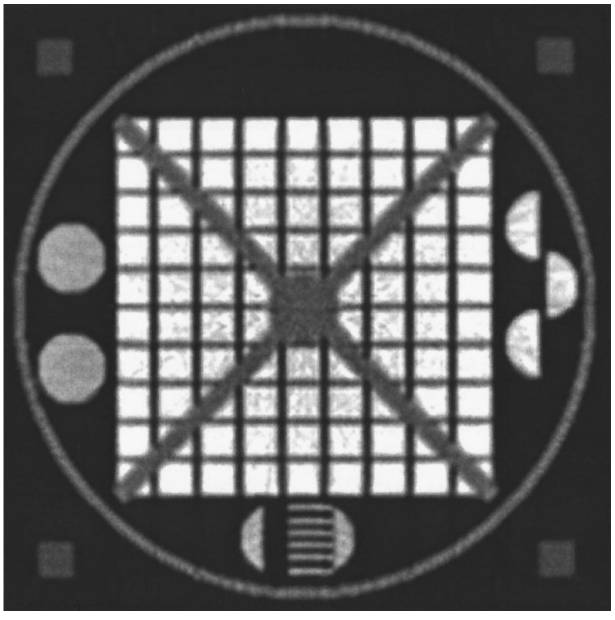

FIG. 2—*Continued*

corrupted by the presence of white noise of variance σ^2 and zero mean value. In this case, the power spectrum $N\mathrm{Pw}_{\varphi,i}(\omega)$ is defined as

$$\begin{aligned} N\mathrm{Pw}_{\varphi,i}(\omega) &= \mathrm{R}^2_{\varphi,i} + n^2_{\mathrm{R}_{\varphi,i}} + 2\mathrm{R}_{\varphi,i} \cdot n_{\mathrm{R}_{\varphi,i}} \\ &\quad + \mathrm{I}^2_{\varphi,i} + n^2_{\mathrm{I}_{\varphi,i}} + 2\mathrm{I}_{\varphi,i} \cdot n_{\mathrm{I}_{\varphi,i}} \\ &= \mathrm{Pw}_{\varphi,i} + \mathrm{Pn}_{\varphi,i} + g(\mathrm{Pw}_{\varphi,i}, n_{\varphi,i}), \end{aligned} \quad [7]$$

where $n_{\mathrm{R}_{\varphi,i}}$ and $n_{\mathrm{I}_{\varphi,i}}$ are the noise contained in the real and imaginary parts of the measured projection respectively, $\mathrm{Pn}_{\varphi,i}$ is the power spectrum of the noise (taking into account the noise affecting both real and imaginary parts) and $g(\mathrm{Pw}_{\varphi,i}, n_{\varphi,i})$ is a function including the products between the noise terms and the signal terms. To include the effect of noise in the definition of the entropy of the power spectrum, we can assume that $N\mathrm{Pw}_{\varphi,i}\log(1/N\mathrm{Pw}_{\varphi,i}) = 0$ for $N\mathrm{Pw}_{\varphi,i} \leq 2(m_{\mathrm{pw}} + \sigma_{\mathrm{pw}})$ and for $N\mathrm{Pw}_{\varphi,i} \geq 1/n^2 - 2(m_{\mathrm{pw}} + \sigma_{\mathrm{pw}})$, where m_{pw} and σ_{pw} are the mean value and the standard deviation of the noise (defined by the square of the gaussian noise present in the measured terms, real and imaginary), respectively. The factor 2 is due to the sum of two noise terms, one for the real part and the other for the imaginary part, having the same power value and characteristics. It can be shown that m_{pw} and σ_{pw} are related to the standard deviation of the original noises by the following relationships: $m_{\mathrm{pw}} = \sigma^2$ and $\sigma_{\mathrm{pw}} = \sigma^2\sqrt{3/2\sqrt{\pi} - 1}$. In this way, the terms exclusively due to the noise can be compensated for but not those due to $g(\mathrm{Pw}_{\varphi,i}, n_{\varphi,i})$.

The Adaptive Method

The properties of the entropy function, $E\mathrm{Pw}_{\varphi}$, can be used to build an adaptive criterion that allows the acquisition of a set of projections that, without an a priori knowledge of $f(x,y)$, has the maximum information content. This can allow a significant reduction of acquisition time. The choice of the projections is made during the acquisition process, taking into account the information content of the previous projections. The process starts by measuring the projections at four orientations: 0°, 45°, 90°, and 135°. Then the entropy of the power spectrum of each of these projections is evaluated and the next projection is measured between the two that present the maximum difference in the entropy function. The procedure ends when the difference in $E\mathrm{Pw}_{\varphi}$ is below a given value ε that represents a terminating parameter. The parameter ε is evaluated by collecting a fifth projection at an angle of $4/n$ rad (which represents the theoretical minimum angular distance) from the projection of the four initial projections, which has the maximum entropy of the power spectrum. The details of its derivation will be explained in the next section. This algorithm is very similar to that discussed in (*25*), but the functions calculated to apply the procedure are quite different, as is the format of the data set they used.

In practice, the function used to select the new projection from the ith and $(i + 1)$th is

$$\Delta\mathrm{Inf}_i = \Delta E\mathrm{Pw}_i \cdot \Delta\varphi_i \cdot K_i, \quad [8]$$

where $\Delta E\mathrm{Pw}_i = |E\mathrm{Pw}\varphi_{i+1} - E\mathrm{Pw}\varphi_i|$, $K_i = \max(E\mathrm{Pw}\varphi_{i+1}, E\mathrm{Pw}\varphi_i)$ and $\Delta\varphi_i = |\varphi_{i+1} - \varphi_i|$.

The factor K_i guarantees that at parity of difference in entropy, the algorithm selects angles corresponding to a greater entropy, namely, to more information. The term $\Delta\varphi_i$ guarantees that the angular difference between acquisitions is not too high, reducing the chance that important projections are missed. This could otherwise occur in the proximity of the minima and maxima of the entropy.

An example of the application of the regular acquisition method and of the adaptive method is reported in Fig. 1. In particular, Fig. 1A shows the timing diagrams for the gradients, the radiofrequency signal, and the acquisition sequence when a regular acquisition sequence is used. Only the gradient values related to the values 0, $\pi/4$, $\pi/2$, and $3\pi/4$ are shown. The total number of selected projections is chosen at the beginning of the process, at uniform angular distances. Moreover, the projections are collected for increasing values of the direction angle. Figure 1B shows the timing diagrams for the gradients, the radiofrequency signal, and the acquisition sequence when the adaptive selection method is used. The gradient values reported in Fig. 1B refer to some projections that depend on the shape of the sample, have not been chosen a priori, and have not been acquired for increasing values of the direction angle.

The ε Parameter

The minimum difference ε, at which the process of selection of the projections ends, is determined experimentally

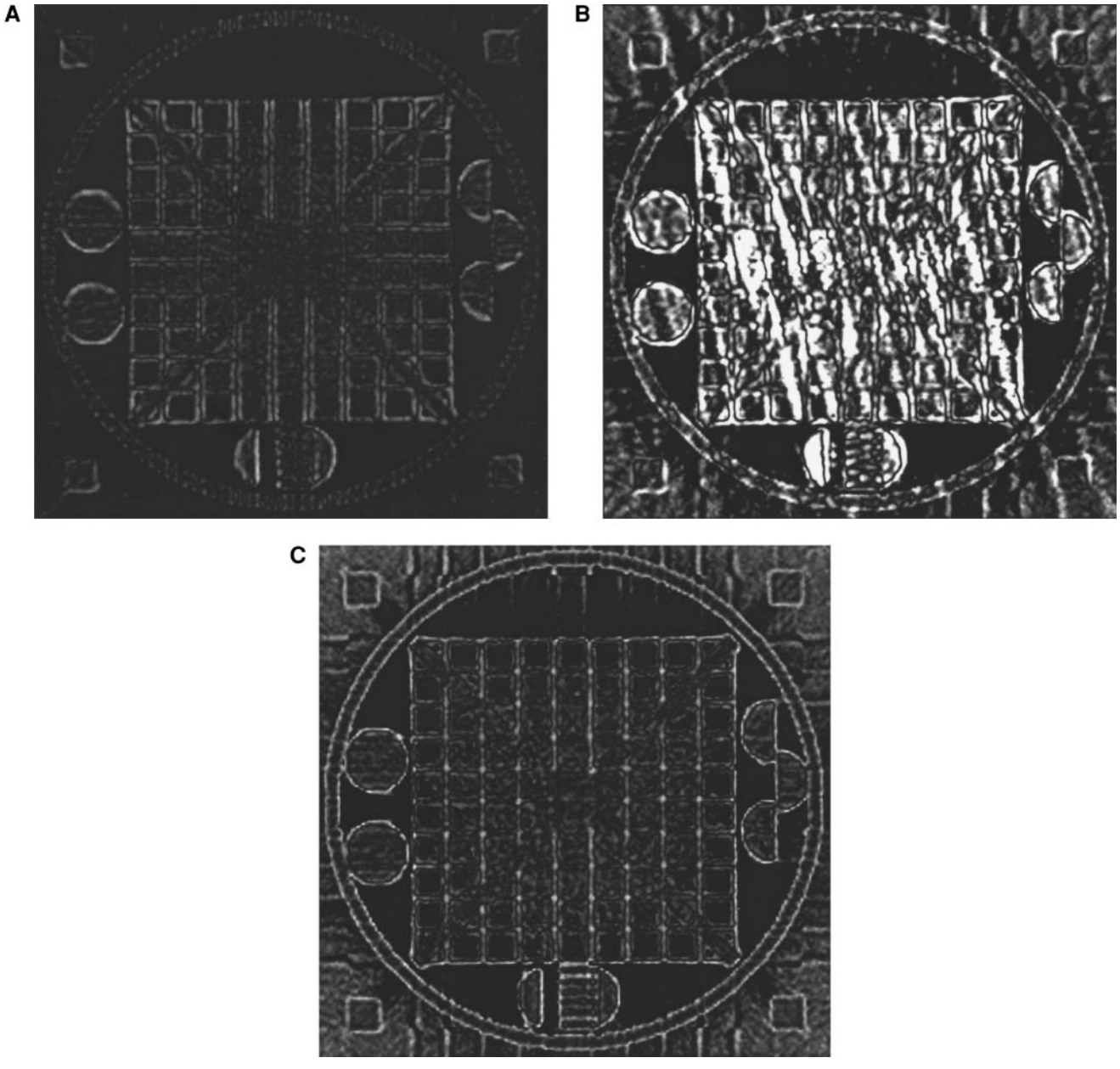

FIG. 3. Difference images from Fig. 2C–Fig. 2B (A), Fig. 2D–Fig. 2B (B), Fig. 2E–Fig. 2B (C) are shown in an expanded grayscale.

by minimizing $\Delta\mathrm{Inf}_i$, evaluated between the projection that has the maximum entropy, of the first four, and the fifth projection measured at $4/n$ rad from it. This is done just before the adaptive acquisition starts. For this purpose, we have to consider that the function $\Delta\mathrm{Inf}_i$ is proportional to the sum of three terms, one accounting for the difference in information between two projections, another being principally due to the noise, and one which is a mixture of signal and noise. In fact, when noise is considered, the expression for $\Delta E\mathrm{Pw}_i$ becomes

$$\begin{aligned}\Delta E\mathrm{Pw}_i = |\sum_{j=1}^{n}\{[\mathrm{Pw}_{\varphi_{i+1},j} + \mathrm{Pn}_{\varphi_{i+1},j} + g(\mathrm{Pw}_{\varphi_{i+1},j},\mathrm{Pn}_{\varphi_{i+1},j})] \\ \times \log(T_{i+1,j}) - [\mathrm{Pw}_{\varphi_i,j} + \mathrm{Pn}_{\varphi_i,j} \\ + g(\mathrm{Pw}_{\varphi_i,j}, \mathrm{Pn}_{\varphi_i,j})] \cdot \log(T_{i,j})\}| \\ = |A + B + C|, \end{aligned} \quad [9]$$

where $\mathrm{Pw}_{\varphi,j}$, $\mathrm{Pn}_{\varphi,j}$ and $g(\mathrm{Pw}_{\varphi,j},\mathrm{Pn}_{\varphi,j})$ are defined as in Eq. [7],

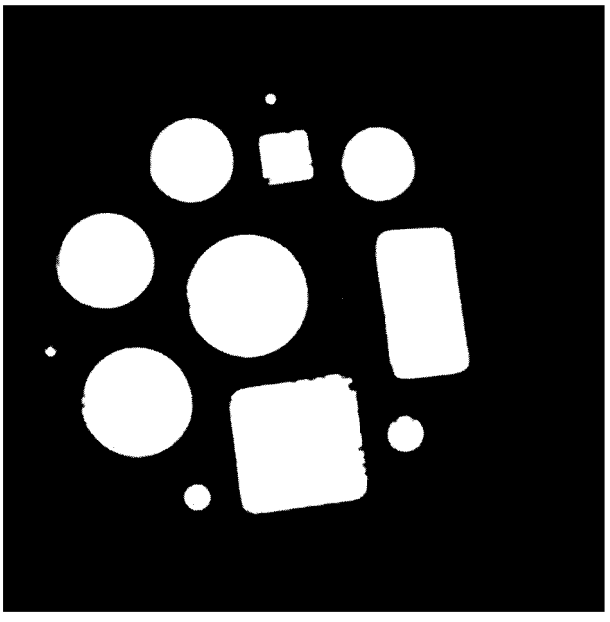

FIG. 4. Transversal MRI reconstruction from projections of a phantom composed of 12 glass tubes filled with water doped with $CuSO_4$. The image has been reconstructed using the whole set of 512 projections and is used as reference image.

$T_{i+1,j} = [1/\mathrm{Pw}_{\varphi_{i+1},j} + \mathrm{Pn}_{\varphi_{i+1},j} + g(\mathrm{Pw}_{\varphi_{i+1},j},\mathrm{Pn}_{\varphi_{i+1},j})]$ and $T_{ij} = [1/\mathrm{Pw}_{\varphi_i,j} + \mathrm{Pn}_{\varphi_i,j} + g(\mathrm{Pw}_{\varphi_i,j},\mathrm{Pn}_{\varphi_i,j})]$, the indices $i + 1$ and i referring to different projections, and the terms A, B, and C are defined as

$$A = \sum_{j=1}^{n}\{\mathrm{Pw}_{\varphi_{i+1},j} \cdot \log(T_{i+1,j}) - \mathrm{Pw}_{\varphi_i,j} \cdot \log(T_{i,j})\} \qquad [10]$$

$$B = \sum_{j=1}^{n}\{\mathrm{Pn}_{\varphi_{i+1},j} \cdot \log(T_{i+1,j}) - \mathrm{Pn}_{\varphi_i,j} \cdot \log(T_{i,j})\} \qquad [11]$$

$$C = \sum_{j=1}^{n}\{g(\mathrm{Pw}_{\varphi_{i+1},j},\mathrm{Pn}_{\varphi_{i+1},j}) \cdot \log(T_{i+1,j}) - g(\mathrm{Pw}_{\varphi_i,j},\mathrm{Pn}_{\varphi_i,j}) \cdot \log(T_{i,j})\}. \qquad [12]$$

The term A is due to the difference between projections, B is essentially due to the noise alone, and C is influenced both by signal and by noise. Lowering of the S/N ratio causes an increase in B and C and as a consequence an increase in the oscillations in $\Delta\mathrm{Inf}_i$, which is the uncertainty of the calculated value of $\Delta\mathrm{Inf}_i$. To set a value for ε which is less influenced by noise, we make the following assumptions. The term K_i of Eq. [8] is taken to be equal to $1/n^2$ which is the minimum value it can assume. The minimum angular distance is taken to be equal to $4/n$ rad. $\Delta E\mathrm{Pw}_i$ is taken to be equal to the difference in entropy between the two considered projections. In this way, we take into account both the minimum angular distance between projections and the minimum difference of entropy between projections. To reduce the noise level in the projections affecting the choice of ε, we subtract from the estimated value of $\Delta E\mathrm{Pw}_i$ an estimated value of B. This is done by substituting in Eq. [11] the level of noise given by $2(m_{\mathrm{pw}} + \sigma_{\mathrm{pw}})$. The term C, as in the case of Eq. [7], cannot be estimated, being a function both of signal and of noise.

The previous definition of ε ensures that the minimum number of projections does not change for different S/N values. In the case of images of complex structure, it approximates to the estimated minimum number of projections, m_0. The number of projections becomes lower when the image has internal symmetries or, being smooth, it is mapped at fewer levels. The use of a conservative value for ε guarantees that the image is reconstructed without any loss of information.

RESULTS

Numerical Results

The ω-space adaptive acquisition method presented here has been tested on simulated data obtained by a 256*256 digital image reported in Fig. 2A. A total set of 1000 FIDs, one per projection, of the phantom was generated using a computer NMR simulation program developed in our laboratory. The program solves the Bloch equations from a map of pixels (the theoretical image) to which cartesian coordinates (positions in centimeters), spin density, main field, and relaxation times values are assigned. The test image was considered 12.8*12.8 cm^2, having a resolution of 0.5 mm. We fixed the main field to 1000 G, $T_1 = 0.8$ s, and $T_2 = 0.16$ s for each pixel. The actions of the pulse sequence and of the gradients are defined in a separate table, called the sequence table. The program calculates the real and imaginary parts of the 1000 FIDs, in steps of 0.18°, in the xy plane of the image, described by using the proper xy gradient combination. To preserve the original dimensions in the reconstructed image, we chose the following acquisition parameters: sampling period 40 ms, sampling rate 6.4 KHz, gradient value 0.12 G/cm, and a rectangular pulse shape of 10 ms in duration. Without loss of generality, the FIDs have been collected considering that the magnetization values are completely recovered between two consecutive experiments (i.e., infinite repetition time). The calculated data set is free from zero-average white noise.

Subsets of different projections were extracted using either the adaptive criterion or the regular acquisition method. A modified Fourier reconstruction algorithm (*26*), including an interpolation method, has been used to obtain the reconstructed images with a low number of projections. The images have been compared both visually and numerically by using the mean square error, MSE, calculated between the image to be tested and the image reconstructed by using the whole set of projections. The comparison with the image obtained with the

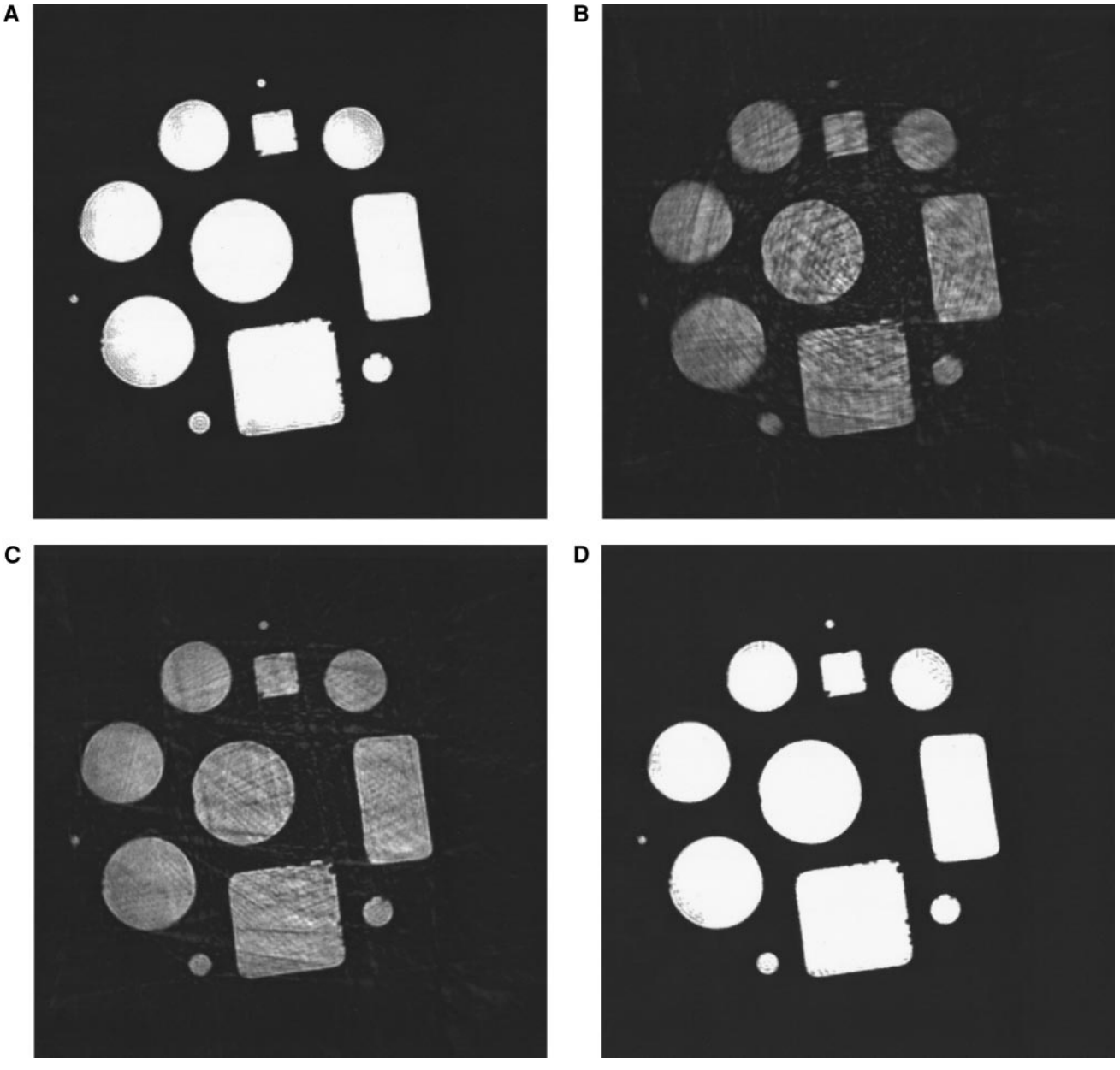

FIG. 5. Images reconstructed by using subsets of projections extracted from the set by which the image of Fig. 3 has been obtained. In particular, the images reconstructed by 57 projections selected by the adaptive method, and by 64, 128, and 256 projections, selected by regular acquisition method, are shown in (A), (B), (C), and (D), respectively.

whole set of projections, and not with the theoretical starting image, is necessary to eliminate the effects of the reconstruction method from the calculated error of the image under inspection. The reference image, obtained by using the whole set of projections, is shown in Fig. 2B. The images obtained by using a set of 120 FIDs, whose orientations are calculated with the adaptive method, and by using a set of 125 FIDs taken at regular angular steps, are shown in Figs. 2C and 2D, respectively. The optimal number of the projections, 120, has also been calculated by the adaptive acquisition method and depends on the shape of the original test image (whose information is collected on the difference between the information content of the projections). The estimated number of projections is about 60% of the minimum number of projections, 201, necessary to reconstruct an image having dimensions and resolution of the given test image, without any a priori information of the sample itself. The image obtained by using the 201 equally spaced projections is also shown in Fig. 2E.

Figure 2D clearly shows some artifacts on both the external and the internal features of the image, due to the low number of projections used in the reconstruction. Nevertheless, Fig. 2C resembles very well the image reported in Fig. 2B, although it

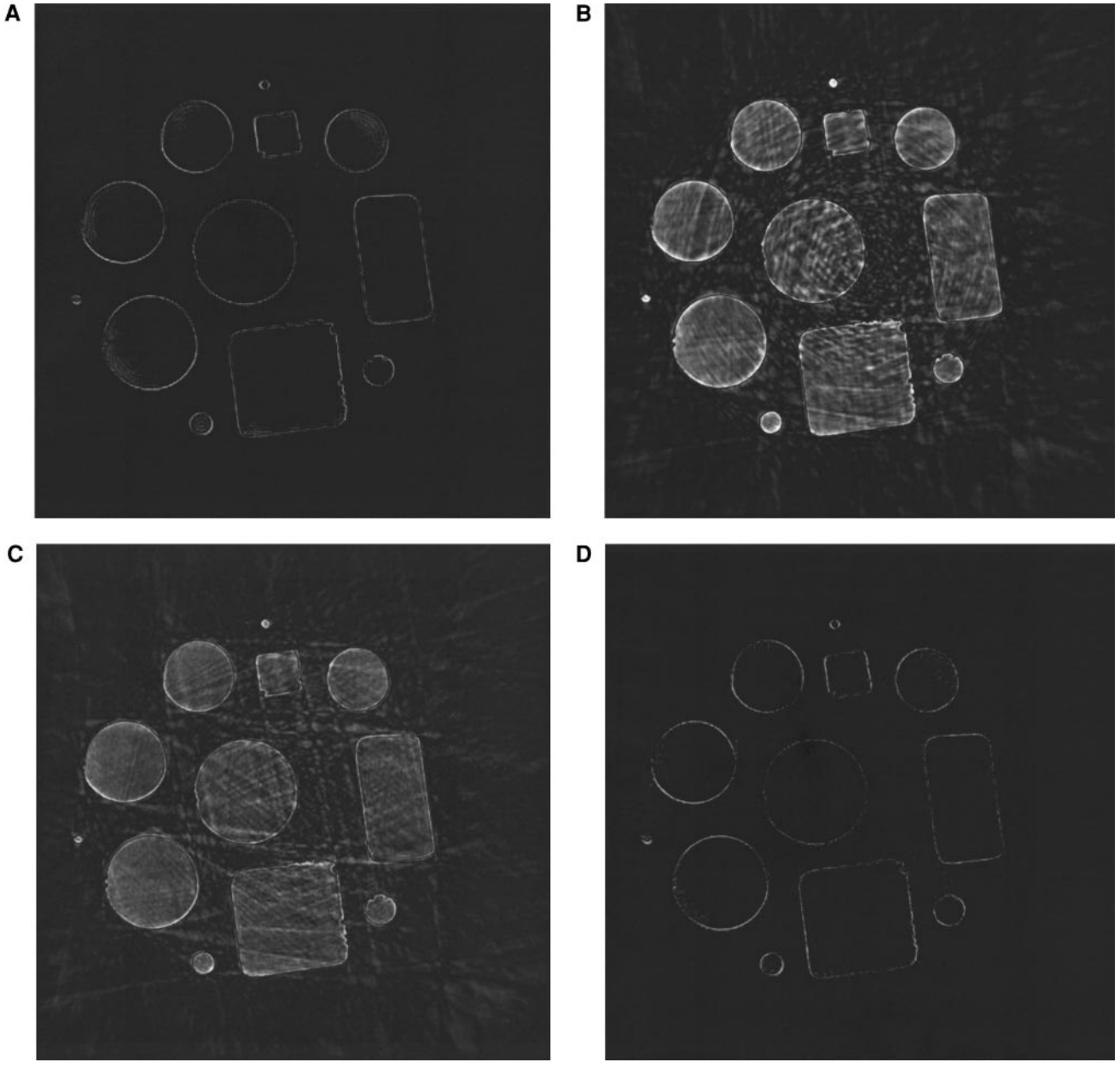

FIG. 6. Difference images from Fig. 5A–Fig. 4 (A), Fig. 5B–Fig. 4 (B), Fig. 5C–Fig. 4 (C), and Fig. 5D–Fig. 4 (A) shown in an expanded grayscale.

is obtained with 12% of the total number of projections and with 5 projections less than the set used to reconstruct Fig. 2D. In particular, Fig. 2C does not show noticeable artifacts because of the optimal choice of the angular positions of the collected projections. The differences between the two images are also evident from the values of the MSE function. In fact, MSE = 0.082 for Fig. 2D and MSE = 0.019 for Fig. 2C, i.e., four times lower. MSE = 0.022 for Fig. 2E; this value is higher than that of Fig. 2C although Fig. 2C has been reconstructed using 120 projections and Fig. 2E with 201 projections. In order to better show the artifacts due to angular undersampling we report in Fig. 3 the difference images in an expanded grayscale.

Experimental Results

The adaptive method has also been tested on MRI experimental data of a phantom composed of a Plexiglas cylinder (internal diameter 4 cm, length 8 cm) containing 12 glass tubes 8 cm in length and of various shapes and dimensions, filled with a 10 mM $CuSO_4$ water solution, coaxial with the principal cylinder. The tubes were of circular section (2 of 0.65 mm, 1 of 1.85 mm, 1 of 2.75 mm, 1 of 6.5 mm, 1 of 7 mm, 1 of 8 mm,

1 of 9 mm, 1 of 10 mm in internal diameter), of rectangular section (11.7 by 6.5 mm), and of square section (1 10*10 by 10 mm and 1 3.5*3.5 mm). The data have been collected using a Varian superconductive MRI instrument, producing a main magnetic field of 4.5 T, using an acquisition from projections sequence. A total of 512 radial projections FIDs (180/512° apart) of a transversal slice, 1 mm thick, were collected. A selection gradient of 1.301G/cm and a total readout gradient of 2.535G/cm were used. Each FID, of 256 points, was acquired in 5 ms (sampling rate 51.2 KHz). The pulse duration was 4 ms and the repetition time was 1 s. The experimental data exhibited a S/N value of about 1000. The resolution achieved in the slice plane was 0.183 mm. The total set of projections was used to obtain the image reported in Fig. 4. This image shows some artifacts, represented by misaligned profiles in some external borders, because the on-resonance condition was not perfectly achieved. Moreover, the image shows some little black holes, especially near the corner of the two square tubes: these are due to some little air bubbles in the tubes. For our purpose, these conditions are not disturbing as we used this image as a reference image, for comparison. From the total set of projections, subsets of projections were extracted by using the regular method and by using the adaptive acquisition process. The optimal number of projections calculated by the adaptive method was 57. Regular sets of projections have been obtained by taking 64, 128, and 256 projections of the total 512 projections. These sets were used to reconstruct the images using the modified Fourier reconstruction algorithm (*26*). The resulting images are reported in Fig. 5. In particular, Fig. 5A shows the image obtained using the adaptive set of 57 projections and Figs. 5B–5D show the images obtained by the regular sets of 64, 128, and 256 projections, respectively. The adaptive estimated number of projections, 57, is about 29% of the minimum number of projections, 201, necessary to reconstruct an image of the required dimensions and resolution when no a priori information about the sample has been used. The image reported in Fig. 5A, although a small number of projections has been used for its reconstruction (11% of the total), resembles very well the image obtained with the total set of projections, reported in Fig. 4. The image of Fig. 5B, on the contrary, exhibits the classical artifacts occurring when a low number of projections is used for reconstruction, although it has been obtained with 12% more projections than those used to collect the image of Fig. 5A. Moreover, although the image shown in Fig. 5C was obtained with more than double the number of regular projections with respect to that reported in Fig. 5A, it also exhibits the effects of the undersampling artifacts. These effects are absent in Fig. 5D, due to the great number of projections used in the reconstruction of this image that exceeds the minimum number required, 201. The good result of the adaptive method with respect to the regular method has been also demonstrated by the difference images reported in Fig. 6 and by the values of the MSE evaluated between the images of Figs. 5 and 4. In particular, Fig. 5A has MSE = 0.28, Fig. 5B has MSE = 0.56, Fig. 5C has MSE = 0.4, and Fig. 5D has MSE = 0.23.

The extremely good performance of the adaptive acquisition method occurs for two reasons: first, it adapts well to the shape of the sample; second, the sample shows a low dynamic range (two amplitude levels) and a relatively simple shape. Nevertheless, comparison with the images obtained by using a regular set of projections shows that, also in the condition of low dynamic range or when the sample exhibits a regular shape, the regular acquisition method fails because it does not use information on the sample. On the contrary, the adaptive method has the great advantage of collecting some information on the sample, starting from the first four measured projections, and of controlling the following acquisition process by measuring the most informative projections.

CONCLUSIONS

In the present work, the information content of an MRI projection directly in the ω-space has been defined. Moreover, a near-optimal RP acquisition method has been described that makes it possible to reduce the total acquisition time, with minimum loss of resolution and the introduction of a few distortions in the resulting image. The method has been tested both on numerical and on experimental data. As shown in the numerical tests reported, the use of the adaptive technique reduces the number of projections to about 60% of the theoretical number of projections required to obtain an image of given dimensions and resolution, saving 40% of the acquisition time. For the experimental test reported, only 29% of the theoretical number of projections was required, saving more than 70% of acquisition time. The results of the adaptive method have also been compared to those of the regular acquisition method: the latter produces artifacts when using a number of projections comparable to that used by the adaptive acquisition method and, for the experimental data presented, also when using more than double the number of projections. The values of the mean square error confirmed the great differences between the two acquisition methods in favor of the adaptive acquisition technique. The good performance of the ω-space adaptive acquisition technique in saving acquisition time in addition to that obtained by RP techniques makes it possible to use this method with success in imaging of species having very short T_2 or in angiography.

In future, we hope to demonstrate that our method works well also when imaging moving objects in order to apply it in functional MRI.

REFERENCES

1. P. C. Lauterbur, *Nature* **242,** 190 (1973).
2. J. G. Pipe and T. L. Chenevert, *Magn. Reson. Med.* **19,** 175 (1991).
3. J. P. Felmlee and R. L. Ehman, *Radiology* **164,** 559 (1987).
4. M. L. Wood and R. M. Henkelman, *Med. Phys.* **13,** 794 (1986).

5. D. R. Bailes, D. J. Gilderdale, G. M. Bydder, A. G. Collins, and D. N. Firmin, Abstracts of the Society of Magnetic Resonance in Medicine, 4th Annual Meeting, p. 939 (1985).
6. J. J. E. Cuppen, J. P. Groen, J. J. E. In Den Kleef, and H. A. Tuithof, Abstracts of the Society of Magnetic Resonance in Medicine, 4th Annual Meeting, p. 962 (1985).
7. P. S. Melki, R. V. Mulkern, L. P. Panych, and F. A. Jolesz, *J. Magn. Reson. Imaging* **1,** 319 (1991).
8. C. H. Meyer and A. Macovski, Abstracts of the Society of Magnetic Resonance in Medicine, 6th Annual Meeting, p. 230 (1987).
9. R. J. Ordidge, R. Coxon, A. Howseman, B. Chapman, R. Turner, M. Stehling, and P. Mansfield, *Magn. Reson. Med.* **8,** 110 (1988).
10. C. J. Bergin, J. M. Pauli, and A. Macovky, *Radiology* **179,** 777 (1991).
11. G. H. Glover and J. M. Pauli, *Magn. Reson. Med.* **28,** 275 (1992).
12. S. L. Gewalt, G. H. Glover, L. W. Hedlund, G. P. Cofer, J. R. MacFall, and G. A. Johnson, *Magn. Reson. Med.* **29,** 99 (1993).
13. A. F. Gmitro and A. L. Alexander, *Magn. Reson. Med.* **29,** 835 (1993).
14. R. Van de Walle, I. Lemahieu, and E. Achten, *Comp. Med. Imag. Graph.* **22,** 115 (1998).
15. T. Schaffter, V. Rasche, and I. C. Carlsen, *Magn. Reson. Med.* **41,** 954 (1999).
16. Y. Cremillieux, A. Briguet, and A. Deguin, *Magn. Reson. Med.* **32,** 23 (1994).
17. P. Latta, V. Jellus, L. Budinsky, V. Mlinarik, and I. Tkac, Abstracts of the Society of Magnetic Resonance, 3rd Annual Meeting, p. 1182 (1995).
18. J. B. Ra, S. K. Hilal, and Z. H. Cho, *Magn. Reson. Med.* **3,** 296 (1986).
19. J. M. Pauli, S. Conolly, D. Nishimura, and A. Macovski, Abstracts of the Society of Magnetic Resonance in Medicine, 8th Annual Meeting, p. 28 (1989).
20. D. Nishimura, A. Macovski, J. I. Jackson, R. S. Hu, C. A. Stevick, and L. Axel, *Magn. Reson. Med.* **8,** 96 (1988).
21. H. T. C. Nielsen, E. W. Olcott, and D. G. Nishimura, *Magn. Reson. Med.* **37,** 285 (1997).
22. L. D. Hall and S. Sukumar, *J. Magn. Reson.* **56,** 179 (1984).
23. V. Rasche, R. W. deBoer, D. Holz, and R. Proksa, *Magn. Reson. Med.* **34,** 754 (1995).
24. R. A. Brooks and G. Di Chiro, *Phys. Med. Biol.* **21,** 689 (1976).
25. G. Placidi, M. Alecci, and A. Sotgiu, *J. Magn. Reson. B* **108,** 50 (1995).
26. G. Placidi, M. Alecci, S. Colacicchi, and A. Sotgiu, *J. Magn. Reson.* **134,** 280 (1998).